The Boris-Algorithm in Practice

Working Paper · February 2017

DOI: 10.13140/RG.2.2.23059.89127

1 author:

Horst Jürgen Andrä
University of Münster
146 PUBLICATIONS **2,072** CITATIONS

SEE PROFILE

The Boris-Algorithm in Practice

H.J. Andrä,

Former member of the Inst. für Kernphysik, Univ. Münster, Wilhelm Klemm Str. 9, D-48149 Münster, Germany

Abstract. The Boris-algorithm is adapted to the realistic gyrating motion of charged particles in strong magnetic fields. This includes the procedures for the change of time-steps from Δt to Δt' as well as those for the correct description of collisions with other charged particles. With these procedures examples of simulations of electrons in Electron-Cyclotron-Resonance-Ion-Sources are shown and discussed.

A) Introduction

The intriguing accuracy and stability of the Boris-algorithm [1, 2] is still stimulating profound mathematical investigations [3, 4]. Its practical application allows the three-dimensional simulation of relativistic electrons in complex Minimum-B Magnetic Structures (MBMS). The most used MBMS are those in Electron Cyclotron Resonance Ion Sources (ECRIS) which are well described in Geller's compendium [5]. These MBMS are created by two symmetric well separated axial magnetic mirror coils superimposed by a long radial n-pole which is usually a n=3-hexa-pole. From our laboratory [6-13] two examples of relatively weak and small MBMS are presented in Fig.1.

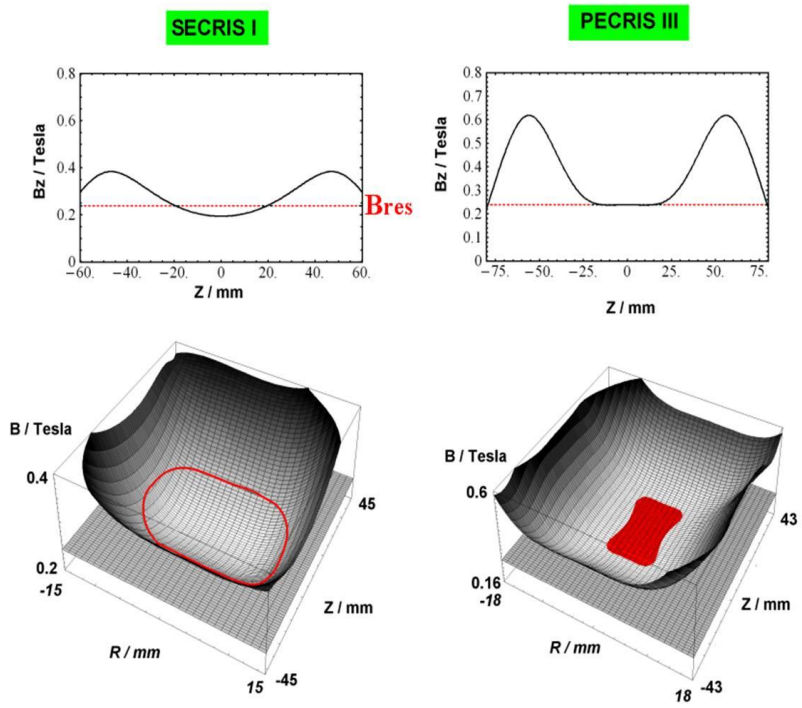

Fig.1 In the upper part: The magnetic field on axis. On the left with a parabolic minimum as used in most Standard ECRIS (SECRIS). On the right with a flat minimum as used in some highly efficient Plateau ECRIS (PECRIS). In the lower part: On the left a typical parabolic minimum of $|\mathbf{B}(\mathbf{r})|$ in a SECRIS. On the right the flat minimum or plateau $|\mathbf{B}(\mathbf{r})|$ in a PECRIS.

The force $\mathbf{F}=\mathrm{grad}(\boldsymbol{\mu}\cdot\mathbf{B})$ drives charged particles back towards the minimum in the center. (Note that $\boldsymbol{\mu}$ of gyrating particles is anti-parallel to $\mathbf{B}$ so that $\mathbf{F}$ is proportional to –grad(B).) This force in a MBMS of an ECRIS does allow the continuous operation of these ECRIS over weeks.

Inside these ECRIS exist the only known stable high energy plasmas with average electron energies of up to hundreds of keV or of billions of Kelvin.

Despite the smooth minima of $|\mathbf{B}(\mathbf{r})|$ in Fig.1 the vector fields in these ECRIS are much more complex as shown in Fig.2 for the PECRIS III of Fig.1. Since only field lines are shown which start at a cylinder close to the axis, the distribution of field vectors $\mathbf{B}(\mathbf{r})$ is still more complex. A presentation of $\mathbf{B}(\mathbf{r})$ in two planes, separated by 60 degrees in Fig.3 gives a further impression of this complexity.

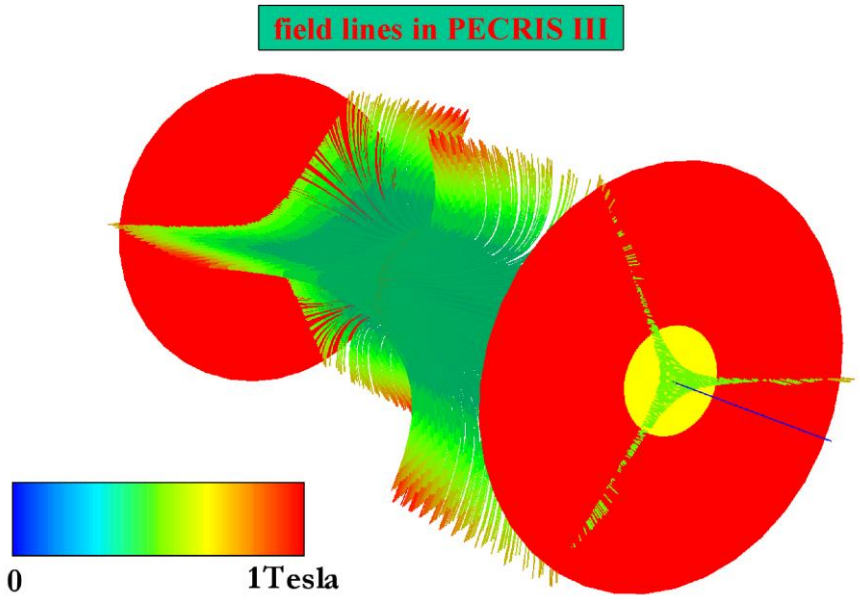

Fig.2 Magnetic field lines in PECRIS III of Fig.1 starting from a cylinder close to the axis.

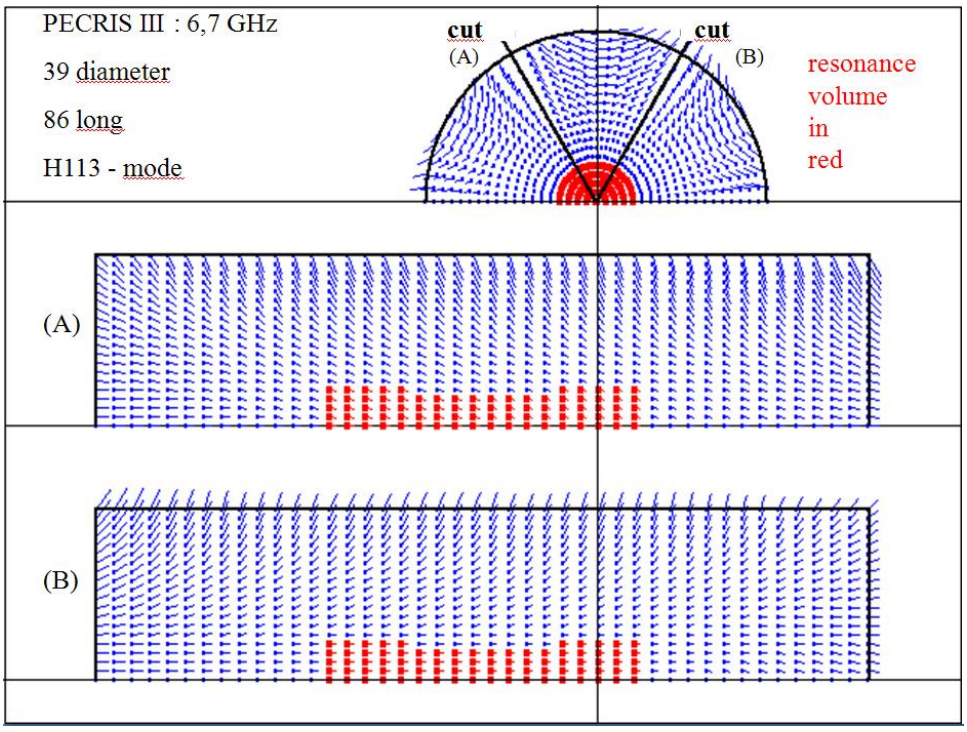

Fig.3 Magnetic field vectors in PECRIS III in two planes of cuts (A) and (B), separated by 60 degrees. The vectors start at the points and follow the lines, the lengths of which are the absolute values of $\mathbf{B}(\mathbf{r})$.

In addition to this complex static magnetic structure the electrons are exposed to an electro-magnetic micro-wave field with frequency ω. It is in resonance with gyrating electrons on a hyper-surface $\left|B_{res}(\underline{\mathbf{r}}, E_{kin})\right| = \left|(\omega m_0/e)(1+E_{kin}/m_0c^2)\right|$=const. Evidently this hyper-surface spatially changes when the electrons gain or lose kinetic energy E_{kin}. This hyper-surface for E_{kin}=0 is shown in red on the left of Fig.1 for a SECRIS and at the right of Fig.1 for a PECRIS. The much bigger hyper-surface in a PECRIS immediately explains the high Electron Cyclotron Resonance (ECR) Heating (ECRH) efficiency of these PECRIS. This high efficiency is, however, only obtained when they are run with several frequencies ω_k in order to further accelerate electrons of k groups of kinetic energy.

From a general physics point of view microwave-energy is pumped via ECRH only into the electronic component of the plasma and stays there until the electrons deliver it to the walls. Due to the great difference in mass the electrons can only transfer a negligible amount of energy to the neutralizing ions. In addition only a negligible amount of the electronic energy is used to ionize neutrals and ions. With nearly all energy in the electronic component of the plasma the spatial and energy distributions of the electrons determine the behavior of an ECRIS by producing and housing the ions in these distributions. It is thus of primordial importance to well understand the electrons in such plasma including their collisions amongst themselves and with the ions before considering any collective plasma phenomena. The near perfect decoupling of the electrons from the ions therefore does not require the use of plasma physics codes, the major goal of which is the correct incorporation of the electron-ion interaction and of collective phenomena in thermal plasmas. Therefore the calculation of trajectories of single electrons can be performed in these complex magnetic structures under ECRH-conditions. They can provide the Spatial Density Distribution (SDD) and the Spatial Energy Density Distribution (SEDD) in ECRIS [6-13]. The best known algorithm is required for this purpose which can cope with massive field gradients and with the ECR-interaction in strong magnetic fields. According to Refs.[3, 4] the Boris-algorithm [1, 2] for relativistic, gyrating particles is the best choice.

B) Adaptation of the Boris-algorithm in practice

The Boris-algorithm [1, 2] is particularly well adapted to the motion of charged particles in constant magnetic fields, but can also handle spatially or temporarily varying magnetic and electric fields. The high efficiency of the Boris-algorithm relies on the exact mathematical reproduction of the physical orbit by straight line elements which we may call Boris-orbit.

For $\underline{\mathbf{B}}(\underline{\mathbf{r}}_1,t_1)=(0,0,B_z)$ and $\underline{\mathbf{E}}(\underline{\mathbf{r}}_1,t_1)=0$ the line element from $\underline{\mathbf{r}}_1$ to $\underline{\mathbf{r}}_2$ in Fig.4 has exactly the same length $\underline{\mathbf{v}}_{12\perp}\Delta t$ as the corresponding arc $R_{phys}\Delta\varphi$ of the physical orbit from $\underline{\mathbf{s}}_1$ to $\underline{\mathbf{s}}_2$. The vector $\underline{\mathbf{v}}_{12\perp}$ is the projection of the vector $\underline{\mathbf{v}}_{12}$ on a plane perpendicular to $\underline{\mathbf{B}}(r_1,t_1)$. With the cyclotron frequency $\omega=(eB/m_0)\sqrt{(1-v_{12}^2/c^2)}$, $\omega R_{phys}=v_{12\perp}=v_\perp=\left|[\underline{\mathbf{v}}_{12}\times\underline{\mathbf{B}}(\underline{\mathbf{r}}_1,t_1)]\right|/B(\underline{\mathbf{r}}_1,t_1)$. These definitions guarantee the energy conservation of the algorithm for step sizes $0<\Delta\varphi<\pi$ (!) and allow with $R_{min}<R_{phys}<R_{math}$ the near perfect reproduction of the orbit for $\Delta\varphi<\pi/9$ which are huge step sizes with respect to other algorithms. R_{math} and R_{min} are easily obtained by geometrical considerations in Fig.4 where $R_{math}\sin(\Delta\varphi/2)=v_{12\perp}\Delta t/2=R_{phys}\Delta\varphi/2$ and $R_{min}=R_{math}\cos(\Delta\varphi/2)$. The only limitations on the step size are imposed by $\underline{\mathbf{B}}(\underline{\mathbf{r}}_1,t_1)\neq\underline{\mathbf{B}}(\underline{\mathbf{s}}_1,t_1)$ and $\underline{\mathbf{E}}(\underline{\mathbf{r}}_1,t_1)\neq\underline{\mathbf{E}}(\underline{\mathbf{s}}_1,t_1)$ when significant variations of the magnetic or electric fields exist over spatial distances $R_{math}-R_{phys}=R_{phys}((\Delta\varphi/2)/\sin(\Delta\varphi/2)-1)$.

For the general case of $\underline{\mathbf{B}}(\underline{\mathbf{r}}_2,t_2)\neq0$ and $\underline{\mathbf{E}}(\underline{\mathbf{r}}_2,t_2)\neq0$ one step from $\underline{\mathbf{r}}_2$ to $\underline{\mathbf{r}}_3$ of the Boris-particle-mover consists of the following operations which assume $\underline{\mathbf{v}}_{12}$, $\underline{\mathbf{r}}_2$, and t_2 to be known from the

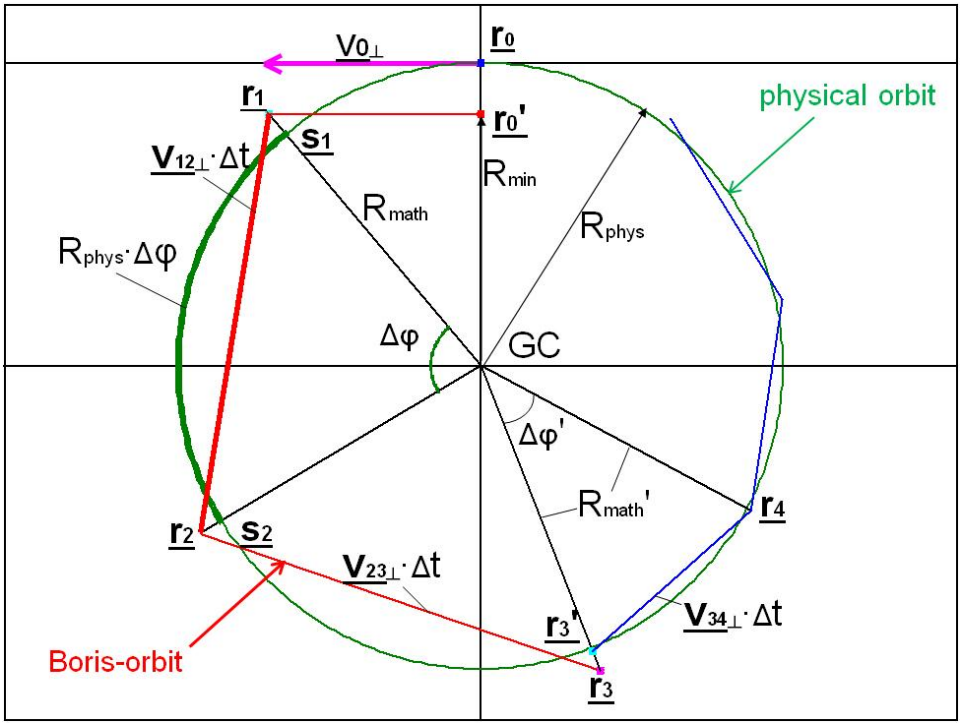

Fig.4 See text.

previous step. The proper velocity $\underline{\mathbf{u}}_{12}$ is used for convenience of the relativistic description of the dynamics.

$$\underline{\mathbf{u}}_{12}=\underline{\mathbf{v}}_{12}/\sqrt{(1-v_{12}^2/c^2)} \quad (1)$$

$$\underline{\mathbf{u}}'=\underline{\mathbf{u}}_{12}+(qe\underline{\mathbf{E}}(\underline{\mathbf{r}}_2,t_2)/m_0)\Delta t/2 \quad (2)$$

$$\underline{\mathbf{u}}''=(\text{rotation of } \underline{\mathbf{u}}' \text{ around } \underline{\mathbf{B}}(\underline{\mathbf{r}}_2,t_2) \text{ by } \Delta\varphi) \quad (3)$$

$$\underline{\mathbf{u}}_{23}=\underline{\mathbf{u}}''+(qe\underline{\mathbf{E}}(\underline{\mathbf{r}}_2,t_2)/m_0)\Delta t/2 \quad (4)$$

$$\underline{\mathbf{v}}_{23}=\underline{\mathbf{u}}_{23}/\sqrt{(1-u_{23}^2/c^2)} \quad (5)$$

$$\underline{\mathbf{r}}_3=\underline{\mathbf{r}}_2+\underline{\mathbf{v}}_{23}\Delta t \quad (6)$$

$$t_3=t_2+\Delta t \quad (7)$$

The symmetric application of the electric field interaction via two half steps assures the proper velocity $\underline{\mathbf{u}}'(t_2+\Delta t/2)$ to be rotated which is the proper velocity midway on the arc of the step. This is important for the reversibility of the algorithm which is considered as a quality criterion of an algorithm [2]. Since the velocity vectors used in these expressions can have important z-components, the vector-rotation of $\underline{\mathbf{u}}'$ around $\underline{\mathbf{B}}(\underline{\mathbf{r}}_2,t_2)$ has to be used.

$$\underline{\mathbf{u}}''=\underline{\mathbf{u}}'\cos(\Delta\varphi)+(1-\cos(\Delta\varphi))(\underline{\mathbf{u}}'\cdot\underline{\mathbf{B}})/B^2+\sin(\Delta\varphi)[\underline{\mathbf{B}}\times\underline{\mathbf{u}}']/B \quad (8)$$

When a particle is started at $\underline{\mathbf{r}}_0$, t_0 with $\underline{\mathbf{v}}_0$ it is evident from Fig.4 that the physical starting point has to be shifted by $\underline{\Delta\mathbf{r}}_0=\underline{\mathbf{F}}/F(R_{phys}-R_{min})$ along the vector of the central force $\underline{\mathbf{F}}=qe[\underline{\mathbf{v}}_0\times\underline{\mathbf{B}}(\underline{\mathbf{r}}_0,t_0)]$ from $\underline{\mathbf{r}}_0$ to $\underline{\mathbf{r}}_0'$ for a correct start of the Boris-orbit. R_{phys} and R_{min} have to be calculated with $v_{0\perp}$ as outlined above for $v_{12\perp}$. The first action of the particle mover has then to be a half step with the operations

$$\underline{\mathbf{u}}_0=\underline{\mathbf{v}}_0/\sqrt{(1-v_0^2/c^2)} \quad (9)$$

$$\underline{\mathbf{u}}'=\underline{\mathbf{u}}_0+(qe\underline{\mathbf{E}}(\underline{\mathbf{r}}_0,t_0)/m_0)\Delta t/2 \quad (10)$$

$$\underline{\mathbf{v}_{01}} = \underline{\mathbf{u}'}/\sqrt{(1-u'^2/c^2)} \quad (11)$$

$$\underline{\mathbf{r}_1} = \underline{\mathbf{r}_0}' + \underline{\mathbf{v}_{01}}\Delta t/2 \quad (12)$$

$$t_1 = t_0 + \Delta t/2. \quad (13)$$

From t_1 onwards the particle mover (1) to (7) can be used with constant Δt up to the time t where either $\Delta\varphi=\omega(t)\Delta t$ or $\Delta s=v(t)\Delta t$ have become considerably larger or smaller than the preset values $\Delta\varphi_0$ or Δs_0, like $\Delta\varphi_0=\pi/9$ or $\Delta s_0=0.1$mm, depending on the spatial variations of the fields involved in comparison to the size of the actual orbit. A change from Δt to a new value $\Delta t'$ can be used to improve either the precision of the trajectory or the speed of the calculation depending on whether $\Delta t'$ is shorter or longer than Δt, respectively.

The modification of Δt to a smaller $\Delta t'<\Delta t$ for instance, implies a modification of R_{math} to $R_{math}'< R_{math}$ and R_{min} to $R_{min}'>R_{min}$ for the same R_{phys} at the time of modification for which we choose here t_3 at which $\underline{\mathbf{v}_{23}}$ and $\underline{\mathbf{r}_3}$ are known. These modifications impose the displacement of $\underline{\mathbf{r}_3}$ to $\underline{\mathbf{r}_3}'$ by the amount $R_{math}(t_3)-R_{math}'(t_3)$ in the direction of the guiding centre (GC) in Fig.4 in order to assure a correct Boris-orbit without displacement of the GC. In order to obtain this direction, the velocity vector $\underline{\mathbf{v}_{23}}$ has to be rotated by $\Delta\varphi/2$ into the tangential direction $\underline{\mathbf{v}_{23}}'$ which then allows to calculate the radial direction $\underline{\mathbf{d}_{GC}}$ towards the GC and thereafter the displacement of $\underline{\mathbf{r}_3}$ to $\underline{\mathbf{r}_3}'$. The switching procedure from Δt to $\Delta t'$ consists thus of the following operations.

$$\underline{\mathbf{v}_{23}}' = (\text{rotation of } \underline{\mathbf{v}_{23}} \text{ around } \underline{\mathbf{B}}(\underline{\mathbf{r}_3},t_3) \text{ by } \Delta\varphi/2) \quad (14)$$

$$\underline{\mathbf{d}_{GC}} = (q/|q|)[\underline{\mathbf{v}_{23}}' \times \underline{\mathbf{B}}(\underline{\mathbf{r}_3},t_3)]/(v_{23}'B(\underline{\mathbf{r}_3},t_3)) \quad (15)$$

$$v_{23}\perp' = v_{23}' \left| \underline{\mathbf{d}_{GC}} \right| \quad (16)$$

$$R_{phys} = (m_0 v_{23}\perp'/e\, B(\underline{\mathbf{r}_3},t_3))\sqrt{(1-v_{23}^2/c^2)} \quad (17)$$

$$R_{math} = R_{phys}\,(\Delta\varphi/2)/\sin(\Delta\varphi/2) \quad (18)$$

$$R_{math}' = R_{phys}\,(\Delta\varphi'/2)/\sin(\Delta\varphi'/2) \quad (19)$$

$$\underline{\mathbf{r}_3}' = \underline{\mathbf{r}_3} + \underline{\mathbf{d}_{GC}}(R_{math}(t_3)-R_{math}'(t_3)) \quad (20)$$

Since $\underline{\mathbf{v}_{23}}'$ is a tangential velocity, one has to use in the first step of the now following series of normal Boris-steps a rotation by only $\Delta\varphi'/2$:

$$\underline{\mathbf{u}_{23}}' = \underline{\mathbf{v}_{23}}'/\sqrt{(1-v_{23}^2/c^2)} \quad (21)$$

$$\underline{\mathbf{u}'} = \underline{\mathbf{u}_{23}}' + (qe\underline{\mathbf{E}}(\underline{\mathbf{r}_3},t_3)/m_0)\Delta t'/2 \quad (22)$$

$$\underline{\mathbf{u}''} = (\text{rotation of } \underline{\mathbf{u}'} \text{ around } \underline{\mathbf{B}}(\underline{\mathbf{r}_3},t_3) \text{ by } \Delta\varphi'/2) \quad (23)$$

$$\underline{\mathbf{u}_{34}} = \underline{\mathbf{u}''} + (qe\underline{\mathbf{E}}(\underline{\mathbf{r}_3},t_3)/m_0)\Delta t'/2 \quad (24)$$

$$\underline{\mathbf{v}_{34}} = \underline{\mathbf{u}_{34}}/\sqrt{(1-u_{34}^2/c^2)} \quad (25)$$

$$\underline{\mathbf{r}_4} = \underline{\mathbf{r}_3} + \underline{\mathbf{v}_{34}}\Delta t' \quad (26)$$

$$t_4 = t_3 + \Delta t' \quad (27)$$

All further Boris-steps have to use full rotations by $\Delta\varphi'$ around $\underline{\mathbf{B}}(\underline{\mathbf{r}},t)$.

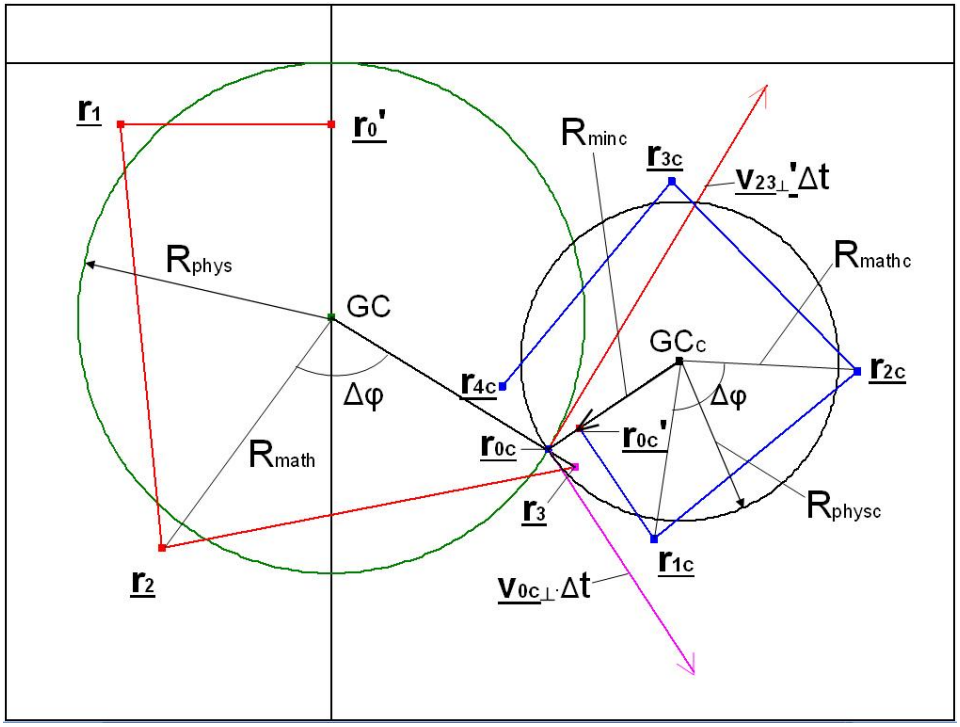

Fig.5 See text.

Collisions require special geometric considerations as indicated in Fig.5. Since a collision represents a sudden change of the velocity vector of a particle on its physical orbit, one has to switch from the Boris-orbit with GC onto the physical orbit, make the collision, and then switch back to a new Boris-orbit with the new GC. In Fig.5 a collision is assumed to take place when the Boris-orbit arrives with $\underline{\mathbf{v}_{23}}$ at $\underline{\mathbf{r}_3}$, t_3. In physical reality, however, the collision takes place with $\underline{\mathbf{v}_{23}'}$ at $\underline{\mathbf{r}_{0c}}$, t_3 where $\underline{\mathbf{v}_{23}'}$ is obtained by (28).

$$\underline{\mathbf{v}_{23}'} = (\text{rotation of } \underline{\mathbf{v}_{23}} \text{ around } \underline{\mathbf{B}}(\underline{\mathbf{r}_3},t_3) \text{ by } \Delta\varphi/2\ ) \qquad (28)$$

$$\underline{\mathbf{d}_{3GC}} = (q/\,|\,q\,|\,)[\,\underline{\mathbf{v}_{23}'} \mathrm{x} \underline{\mathbf{B}}(\underline{\mathbf{r}_3},t_3)]/\,(v_{23}'B(\underline{\mathbf{r}_3},t_3)) \qquad (29)$$

$$\underline{\mathbf{r}_{0c}} = \underline{\mathbf{r}_3} + \underline{\mathbf{d}_{3GC}}\,(R_{math} - R_{phys}) \qquad (30)$$

This tangential velocity $\underline{\mathbf{v}_{23}}$ allows to calculate the unit-direction $\underline{\mathbf{d}_{3GC}}$ towards GC and then to shift the Boris-point $\underline{\mathbf{r}_3}$ to $\underline{\mathbf{r}_{0c}}$ on the physical orbit. At $\underline{\mathbf{r}_{0c}}$ the collision changes $\underline{\mathbf{v}_{23}'}$ to $\underline{\mathbf{v}_{0c}}$ which is assumed to be the result of large angle scattering with a significant z-component in Fig.5. This velocity $\underline{\mathbf{v}_{0c}}$ is the tangential velocity of a new physical orbit with a new guiding centre GCc. This new orbit has the starting conditions $\underline{\mathbf{r}_{0c}}$, $\underline{\mathbf{v}_{0c}}$, $\underline{\mathbf{B}}(\underline{\mathbf{r}_{oc}}, t_3)$ and $\underline{\mathbf{E}}(\underline{\mathbf{r}_{oc}}, t_3)$ and has to be described by a new Boris-orbit with $R_{physc}(t_3)$, $R_{mathc}(t_3)$, $R_{minc}(t_3)$ and a point of departure $\underline{\mathbf{r}_{0c}'}$. The latter four quantities have to be calculated in the same manner as the equivalent quantities at the departure of the Boris-orbit in Fig.4. The first action of the Boris particle mover has then to be a half step from $\underline{\mathbf{r}_{0c}'}$ to $\underline{\mathbf{r}_{1c}}$ with the corresponding equations (9) to (13) with additional index c.

C) Test of the quality of the Boris-algorithm

This test concerns the drift motion in magnetic field gradients, the Δt-switching procedure, and the ECR-interaction. The procedure for collisions is very hard to test because of the statistical nature of collisions. An artificially imposed reversible collision at point $\underline{\mathbf{r}_{0c}}$ would require a return of the Boris-orbit with index c to a point $\underline{\mathbf{r}_{nc}}$ exactly on the line GC_c-$\underline{\mathbf{r}_{0c}}$. Although feasible in principle, this is very hard to implement and has therefore been omitted.

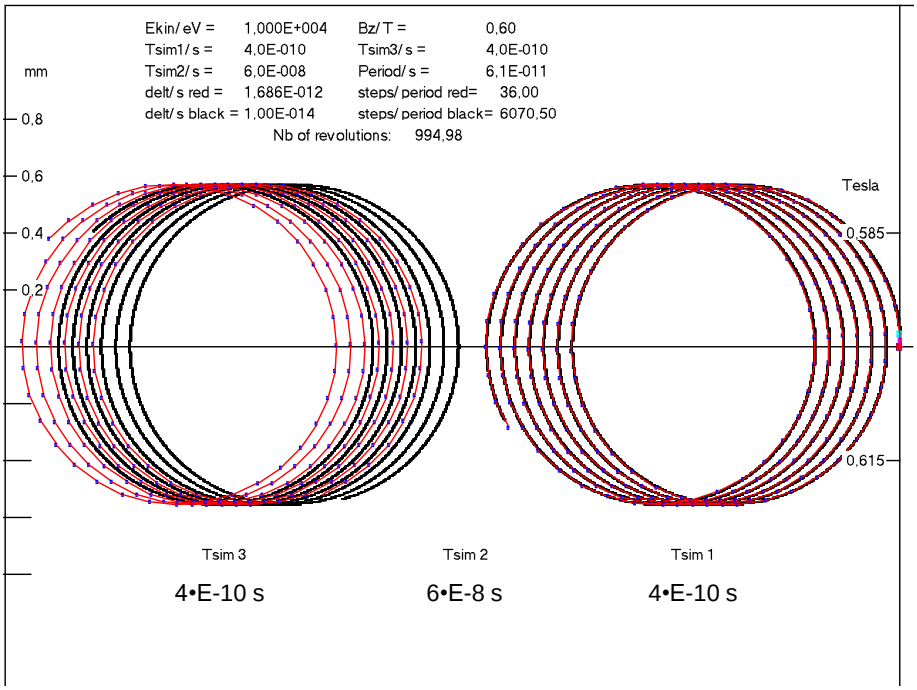

Fig.6 A 10 keV electron starts at the red point with upward velocity. It gyrates in a vertical field gradient of 0.04 T across the orbit. Its drift motion is shown for $T_{sim1}=4\cdot10^{-10}$ s. The further calculation during $T_{sim2}=6\cdot10^{-8}$ s is not shown. The presentation then resumes during another $T_{sim3}=4\cdot10^{-10}$ s.

The number of time-steps per revolution is determined by the correct discrete description of these fields along the orbit of one revolution. A magnetic field gradient of about 0.04 T across an electron orbit (≈3.6 T/m !) at 10 keV at 0.6 T requires 36 time-steps for an orbital shift of only 10% of the diameter after 1000 revolutions in Fig.6 with respect to a supposedly exact calculation with 6070 time-steps per revolution. Therefore 36 time-steps per revolution seem to be an acceptable compromise although 72 time-steps would improve the result considerably at the cost of doubling the time of calculation.

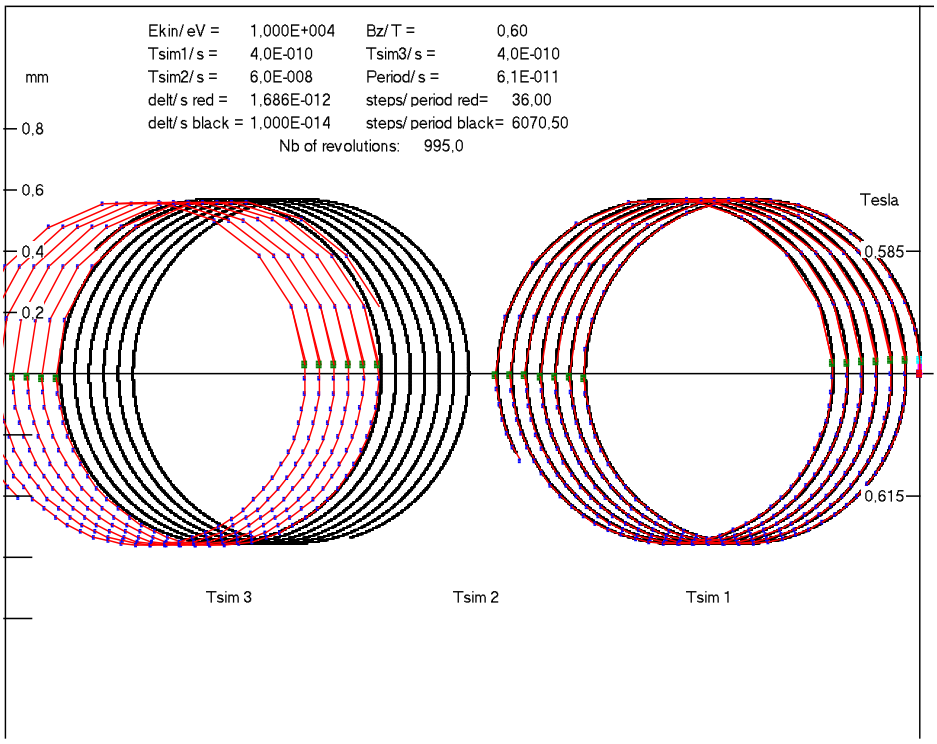

Fig.7 As in Fig.6, but after the first half-revolution a switch from Δt to 4Δt is imposed at the green square on the left of the orbit. After the first complete revolution a switch from 4Δt to Δt is imposed at the green square on the right of the orbit. These two switch-procedures per revolution are imposed during the whole trajectory.

Again the number of time-steps per revolution determines the result in Fig.7. The result in Fig.7 with 72 time-steps in the first half-period and with 18 time-steps in the second half-period is clearly worse than the result in Fig.6. Evidently the half-period with 18 time-steps per period worsens the result more than the improvement expected from the other half-period with 72 time-steps per period. This observation confirms the remarks of above that the description of the field across the orbit is not good enough when about 0.0072 T/step occur during roughly a quarter of a revolution. In practical applications in an ECRIS less than 36 time-steps per revolution have to be avoided.

The algorithm fully takes into account the ECR-interaction whenever oscillating electric field components perpendicular to **B** exist. Depending on the relative phase of such oscillating electric fields with respect to the cyclotron motion of the electron the description of acceleration or deceleration of the electrons will be demonstrated. The gain or loss of E_{kin} is well taken into account with 75 time steps per revolution whenever the electron passes through a spatial region where the resonance condition is fulfilled in Figs.8, 9.

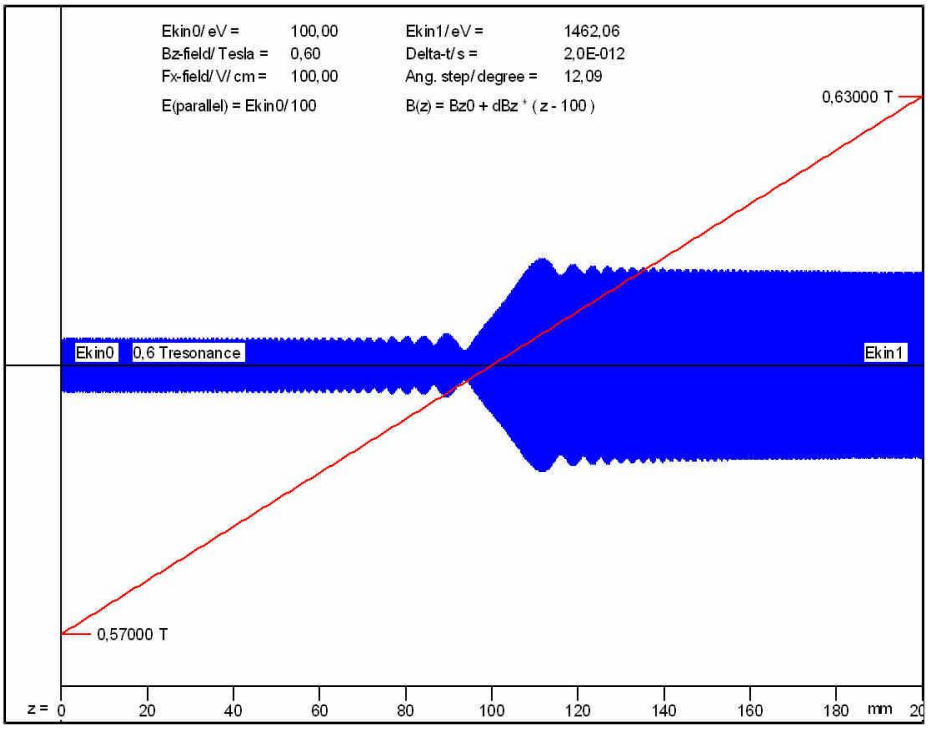

Fig.8 Gain to E_{kin} when an electron of E_{kin0}=100.96eV propagates with an energy of 1eV in the z-direction in a red field B_z which varies from 0.57 T at z=0 to 0.63 T at z=200 mm. The ECR occurs at 0.6 T at z=100 mm with a strong oscillating electric field of 100 V/cm in phase with the gyrating electron. E_{kin1}=1491 eV.

The quality of the simulation of the ECR-interaction is best described by only 1.8% loss of energy gain to 1464 eV when 30 time-steps per revolution are used instead of the 75 in Fig.8. The difference of energy gain and loss in Fig.8 and Fig.9, respectively, confirms the gain of energy $\langle E' \rangle - E_0$ of ECRH when averaging over the phases Θ of the gain of velocity Δv on the orbit when passing through an ECR.

$$\langle E' \rangle - E_0 = \langle \tfrac{1}{2} m(v_0 + \Delta v \cdot \cos\Theta)^2 \rangle - E_0 = \tfrac{1}{4} m \Delta v^2 \qquad (31)$$

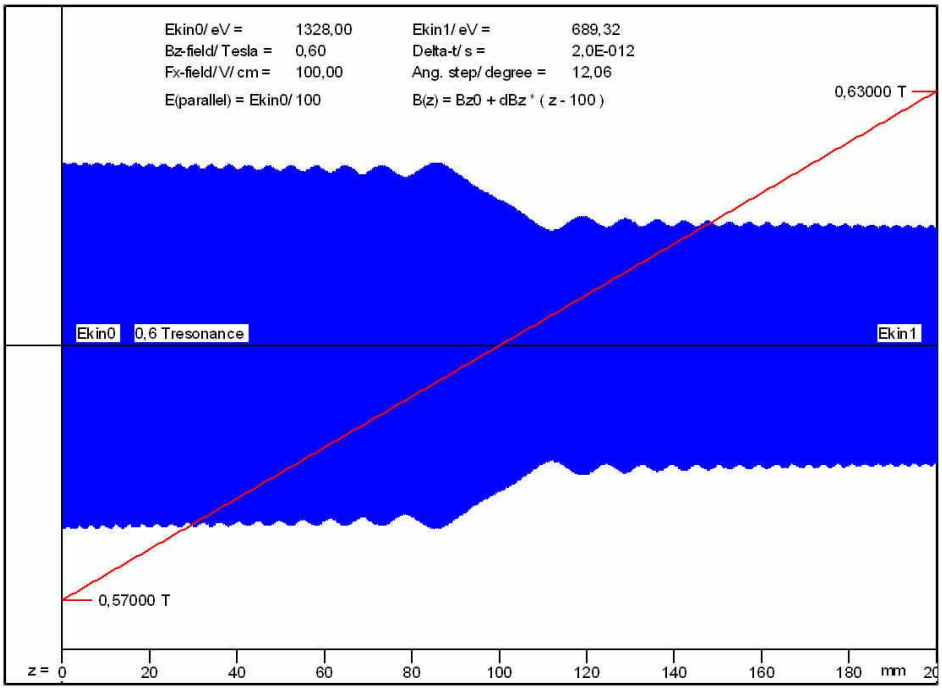

Fig.9 Loss to E_{kin} when an electron of E_{kin0}=1328eV propagates from left to right with 1eV as in Fig.8. It is exposed to a strong oscillating electric field of 100 V/cm in anti-phase with its gyration. E_{kin1}=689 eV.

An important relativistic effect occurs when the electric field strength is increased for the otherwise same conditions. As shown in Figs.10a-d, the energy gain and width of the resonance as defined from the minimum before and the maximum behind the resonance increase systematically with increasing the electric field strength. They seem to diverge when comparing Figs10c and d

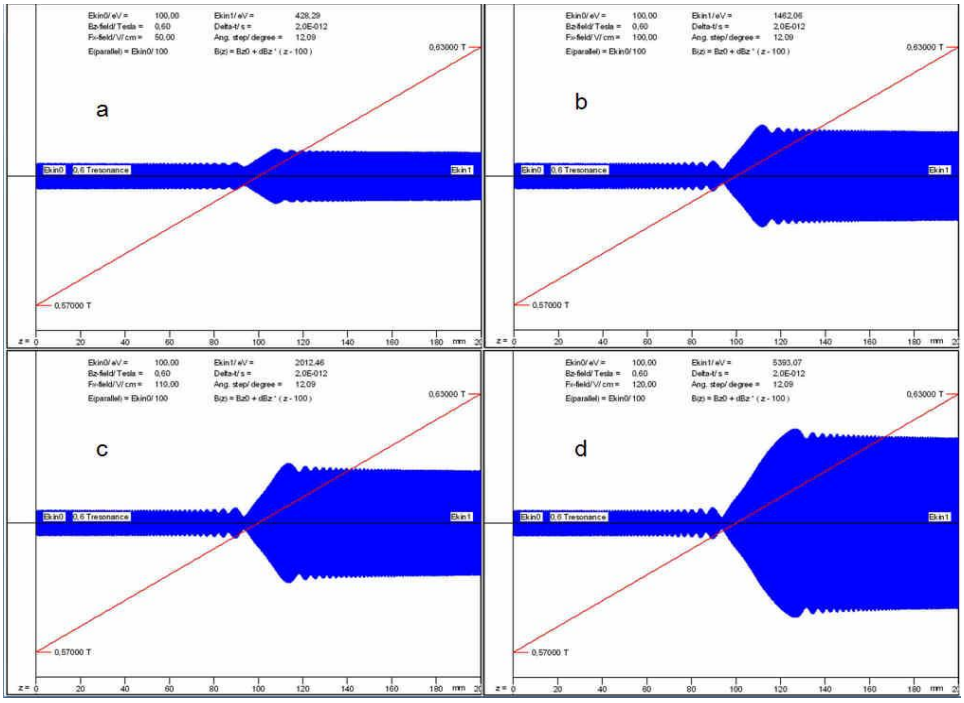

Figs.10a-d Evolution of E_{kin1}[eV] and the width ΔB[T] of the resonance as function of the electric field strength F[V/cm]. a) F=50, E_{kin1}=428, $\Delta B=3.9\cdot10^{-3}$, b) F=100, E_{kin1}=1462, $\Delta B=5.2\cdot10^{-3}$ c) F=110, E_{kin1}=2012, $\Delta B=6.1\cdot10^{-3}$, d) F=120, E_{kin1}=5393, $\Delta B=10.4\cdot10^{-3}$.

which only differ by 5 V/cm whereas ΔB increases from $6.1 \cdot 10^{-3}$ to $10.4 \cdot 10^{-3}$ T. This divergence does indeed occur at only 1 V/cm above the F of Fig.10d as shown in Fig.11. It is due to the increase of the magnetic resonance field $B_{res}(E_{kin})=B_{0res}(1+E_{kin}/m_0c^2)$ (see page 3) with increasing kinetic energy E_{kin} of the electron. During the passage of the electron through the resonance at 0.6 T it gains sufficient energy to be again in resonance at higher magnetic field strength. It is at first out of phase and loses some energy before it regains more energy when being in phase again. Due to the large width of the resonance the loss of energy does not move the electron out of resonance. This periodic relativistic energy gain increases E_{kin1} to some value of saturation far away from the limit of Fig.11. Already at the limit of Fig.11 E_{kin1}= 48830eV and increases further. When the magnetic field gradient is increased by a factor of two, this same divergence occurs at higher field. Also the velocity of the electron from left to right changes the field of divergence. For lower velocities the divergence is shifted to lower F and vice versa. These divergences are expected to produce dramatic effects in any application of resonance heating of electrons when the adequate electric field strengths can be delivered. As the interpretation of these divergences suggests, these divergences do indeed not occur for a negative gradients of the magnetic field. It is furthermore worth noting that Ekin1 stays roughly constant at the right limit of Fig.11 when the field F is further increased up to 600 V/cm.

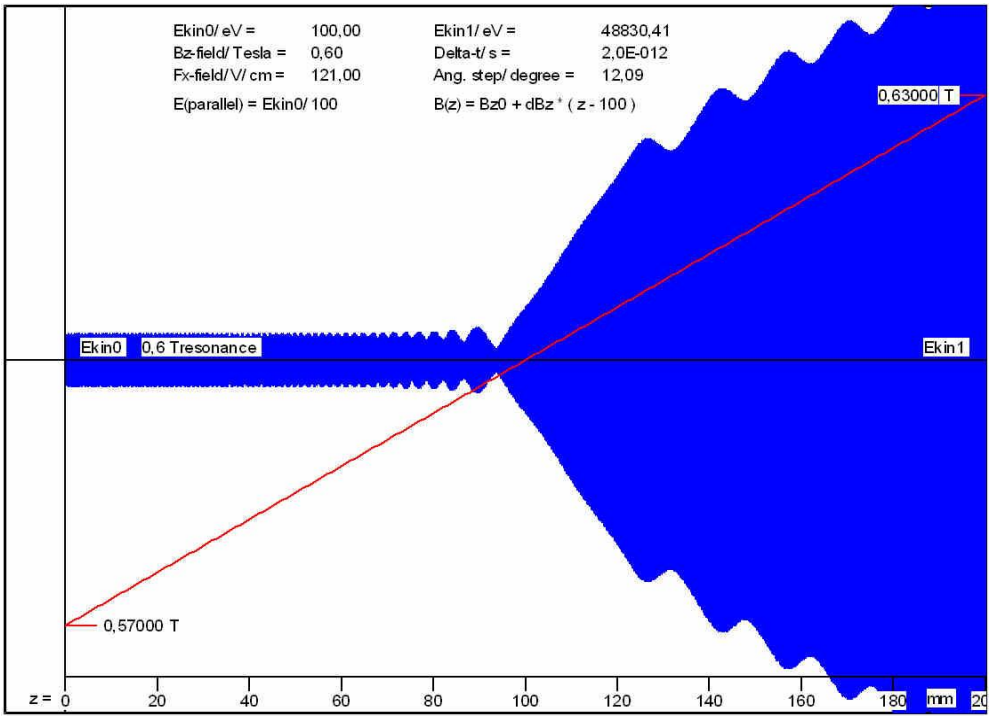

Fig.11 Divergent energy gain at F=121 V/cm for the particular z-velocity of the electron and for the particular linear increase of the magnetic field.

For the lifetime of an electron in an ECRIS the reflection on the magnetic mirrors is of primordial importance. Therefore an electron is started in PECRIS III at z=0 at the radius of the orbit on the x-axis in the y-direction with an energy of 10 keV and with 10eV in the z-direction. As calculated with 36 time-steps per revolution in red it moves in Fig.12 to the right and is reflected at the magnetic mirror during the time of simulation $T_{sim1}=6 \cdot 10^{-9}$ s. Then it bounces back and forth on

axis between the magnetic mirrors on both sides of PECRIS III during the time of simulation T_{sim2}=6·10-6 s which is not shown. Again shown is then the trajectory during a short period of

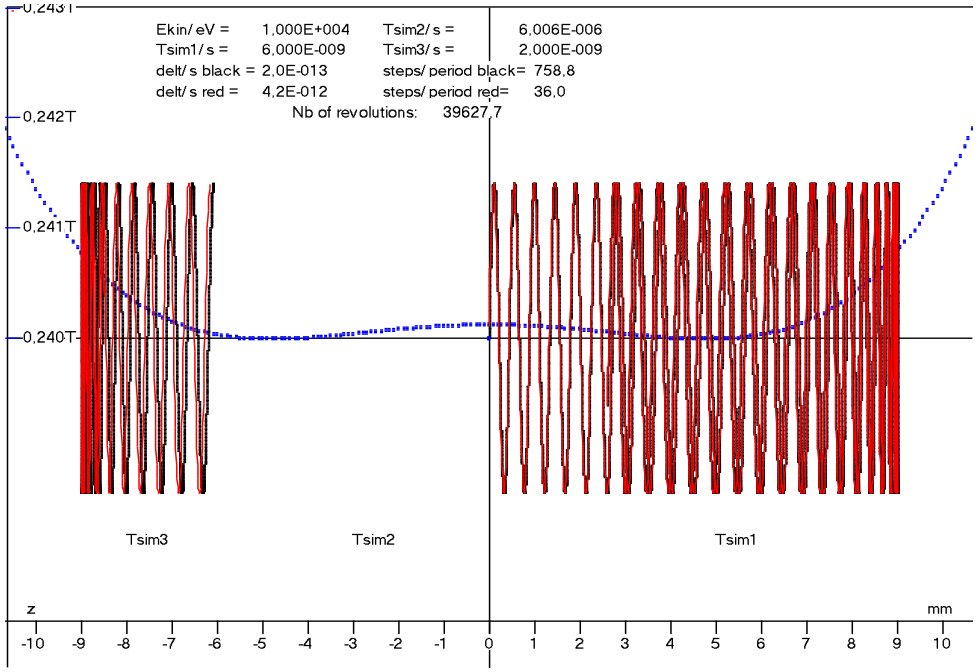

Fig.12 In PECRIS III an electron starts in at z=0 at the radius of the orbit on the x-axis in the y-direction with an energy of 10 keV and with 10eV in the z-direction. The simulation with 36 time-steps per revolution is shown in red on the right during $T_{sim1}=6\cdot10^{-9}$ s. Not shown are then the bounces back and forth on axis during T_{sim2}=6·10-6 s. After $T_{sim}=6.006\cdot10^{-9}$ s the trajectory is shown again during $T_{sim3}=2\cdot10^{-9}$ s. The same simulation is repeated with 760 time-steps per period in black.

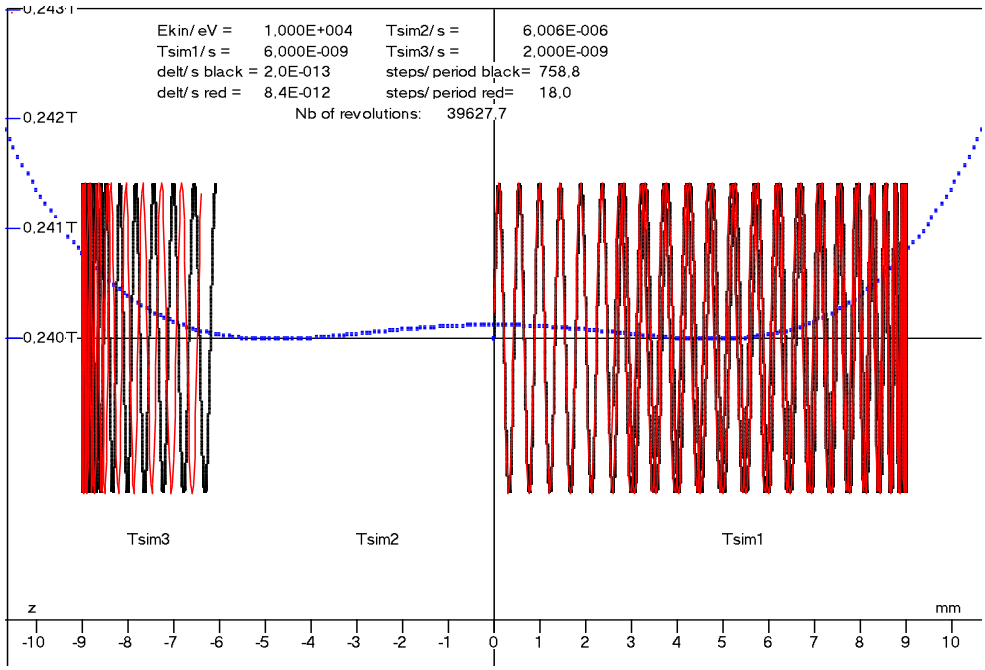

Fig.13 The same simulations as in Fig.12 with 18 time-steps per period in red and with 760 time-steps per period in black.

simulation T_{sim3}= $2\cdot10^{-9}$ s after a total time of T_{sim}=6.006·10-6 s on the left of Fig.12. The comparison with the same simulation with 760 time-steps per period in black shows a very close

agreement after 39628 revolutions. The same simulations with 18 time-steps per period in Fig.13 clearly show a significant loss of precision between the black and the red simulations. 36 time-steps per period are thus an excellent compromise for the simulation of electrons in an ECRIS.

These convincing results demonstrate the excellent efficiency and precision of the Boris-algorithm for the calculation of electron-trajectories in the complex magnetic structures of an ECRIS. As will be shown, this precision of the algorithm results in very precise trajectories with average confinement times of the electrons in PECRIS III of about 0.44 ms and in PECRIS V of about 0.9 ms, i.e. much longer times than in [6-8] despite the full implementation of collisions in our calculations.

D) Simulation of electrons in an ECRIS

A shorthand description of our calculations of the trajectories in an ECRIS has been presented earlier [13]. It shows how the electrons are started, how they and their energy are registered in volume elements during their trajectory, and where and with which energy they hit a wall. These calculations with the Boris-algorithm take into account the collisions of the electrons with other electrons, with differently charged ions, and with neutrals. The description of their implementation in our programs is included in Ref. 10. For the necessary approximations always the worst case has been assumed. Therefore the results also represent the worst case and could in reality be somewhat better.

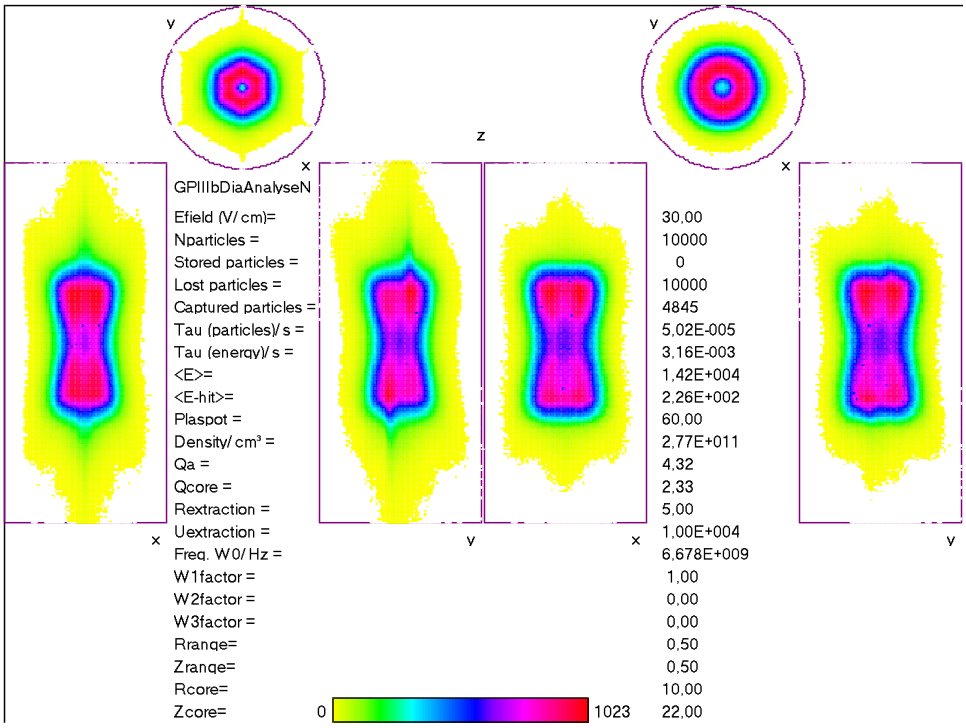

Fig. 14 Spatial density of electrons projected on the z-x- and z-y-planes in the lower left, projected on the x-y-plane in the upper left. Spatial energy density of electrons projected on the same planes in the lower right and on the x-y-plane in the upper right. The color code runs from negligible density in white to the maximum density in red. For more details see text.

Most results of our simulations of various ECRIS are presented in Ref. 10. Here we just show one for PECRIS III as example. PECRIS III has a magnetic confinement as shown on the right of

Fig. 1. A micro-wave power is assumed which produces an electric ECR-field of 30 V/cm of the H_{113}-mode on axis in a cylindrical mono-mode cavity (86 mm long, 39 mm diameter). This cavity is inserted into the magnet field configuration in Figs.1 and 3. The end-caps of this cavity are coated with insulating Al_2O_3 which is supposed to charge up to -60V. Electrons with an energy <60eV are thus reflected at these end-caps. Despite the collisions caused by the high electron density of $2.77 \cdot 10^{11}$ cm^{-3} an average lifetime of the electrons of 50 µs at an average energy of 14.2 keV (~200 million Kelvin !) is obtained. For this result 10^4 electrons survived the starting procedure [13] with 5 eV in arbitrary directions all over the cavity. Their trajectories were pursued until they hit a wall; the longest lifetime observed was 19 ms ! The Spatial Density Distribution (SDD) of the electrons is shown on the left of Fig.14. On the right in the same figure is presented the Spatial-Energy-DD (SEDD). It extends to a slightly greater diameter and length than the DD. This is due to electrons of high energy in the Energy Spectrum (ES) of Fig.16 which climb up the magnetic walls due to relativity as explained above. The spatial confinement of the electrons is thus very good and explains why these ECRIS can run in stable manner during weeks.

Since the SDD and SEDD form a well confined plasma core in the centre of PECRIS III, the escaping electrons and ions form a very sharp impact pattern on the walls in Fig.15. It reproduces exactly the escape channels of the magnetic fields shown in Figs.2 and 3. The walls of the back-side of the cylinder in the upper left and of the extraction-side on the upper right show exactly the same impact pattern as observed in PECRIS III after weeks of operation. The empty circle on the extraction-side is the result of the reflection of the electrons on the potential of 10 kV for the extraction of ions. The lower part is the impact pattern of the simulation on the rolled out wall of the cylinder. It also corresponds to the experimentally observed pattern in PECRIS III.

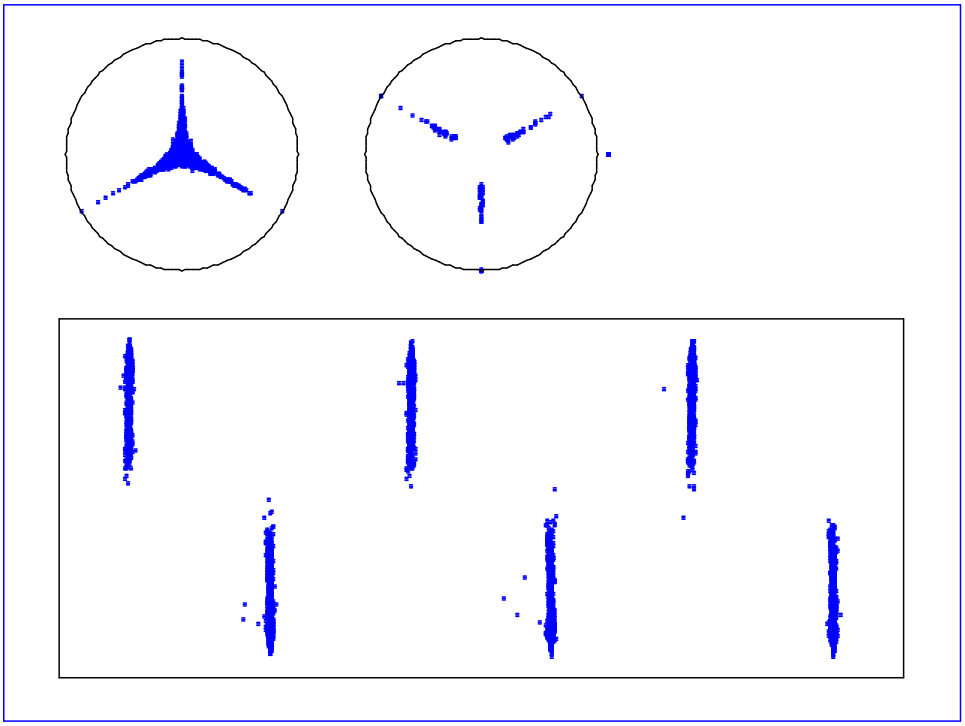

Fig.15 The impact pattern on the walls of the back-side of the cylinder in the upper left and of the extraction-side on the upper right. The lower part is the impact pattern of the simulation on the rolled out wall of the cylinder. For further details see text.

Fig.16 shows the energy spectrum of 10^4 simulated electrons in PECRIS III. The average energy is <E>=14.2 keV and the maximum of energy is E_{max}=80 keV. The energy confinement is excellent since the averaged energy of electrons hitting a wall only is $<E_{hit}>$=226 eV. The electrons with relatively high energy form a very stable dumb-bell shaped negative cloud in the center of PECRIS III. It serves as host for the not heated (E_{ion}<2eV), neutralizing ions which thus also form a very

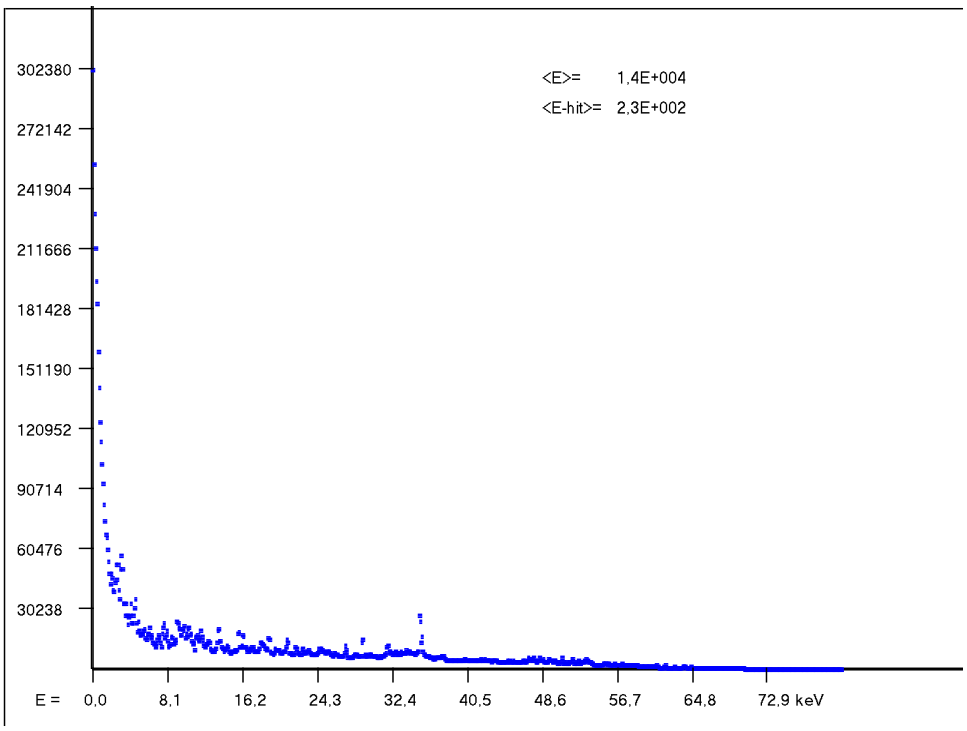

Fig. 16 The energy spectrum of the electrons in PECRIS III.

stable cloud. The lifetime of these ions is long enough for their ionization by the electrons to high charge states. This is the reason why these ECRIS are very efficient reservoirs of highly charged ions. Their extraction from an ECRIS with a negative puller electrode in front of the extraction hole (see the upper right of Fig.15) is not very efficient. Lowering the magnetic mirror on the side of extraction [5, 13] or shifting the whole magnetic structure with respect to the plasma chamber towards the extraction [8, 13] improves the extraction considerably. Another approach is the so called afterglow after a sudden stop of the ECRH [5]. As the simulation [8] shows, the fast moving electrons are then rapidly lost and the cloud of the slowly moving positive ions is left behind so that they Coulomb-explode partially towards the extraction hole, thus forming a short pulse of extracted ions. Instead of switching off the ECRIS, one also can lower the magnetic mirror at extraction during a short pulse [11, 12]. This allows to the highly charged ions to escape towards extraction during this pulse.

E) Conclusion

The Boris-algorithm has proven to be a very efficient tool for the simulation of charged particles in magnetic fields with strong gradients and time-dependent electric fields. It has allowed the simulation of the electrons in such field-configurations in ECRIS [6-13]. These simulations are now a very efficient tool for the understanding of these ECRIS.

F) Acknowledgement

I am indebted to my students L. Müller, G. Leonhardt, A. Heinen, M. Kahnt, C.F. Vitt, B. Albers, M. Rüther, A. Täschner, S. Wolosin, and L. Nowack who provided the Figs.1,2 and who helped me to come closer to an understanding of the Boris-algorithm and of the ECRIS.

G) References

[1] J.P. Boris, in Proc. Fourth Conf. on the Numerical Simulation of Plasmas, p.3 (1970).

[2] C.K.Birdsall and A.B.Langdon, "Plasma Physics via Computer Simulation", IOP-Publishing Ltd.(1995), ISBN 0750301171.

[3] H. Qin et al., Physics of Plasmas **20**, 084503 (2013), and references therein.

[4] C.L. Ellison et al., Journal of Computational Physics **301** (2015), DOI : 10.1016/j.jcp.2015.09.007.

[5] R.Geller, "Electron Cyclotron Resonance Ion Sources and ECR Plasmas", IOP Publishing Ltd. (1966) and 491 references therein, ISBN 0 7503 0107 4.

[6] A. Heinen, M. Rüther, J. Ducrée, J. Leuker, J. Mrogenda, H.W. Ortjohann, Ch. Vitt, E. Reckels, and H.J. Andrä, Rev.Sci.Instr. **69**, 729 (1998), DOI:10.1063/1.1148667.

[7] A. Heinen, Ch. Vitt, and H.J. Andrä, in Conference on the Physics with Highly Charged Ions, Bensheim, Germany Sept. 1998, Physica Scripta **T80**, 517 (1999), http://www.doi.org/10.1238/Physcia.Topical.080a00517.

[8] A. Heinen and H.J. Andrä, Proceedings of the "14th International Workshop on ECR Sources", 3-6 Mai 1999, CERN, Genf, Schweiz, p. 224, http://cern.web.cern.ch/CERN/ Divisions/PS/ECRIS99/Proceedings.html:"Heating and Trapping of Electrons in ECRIS, from Scratch to Afterglow".

[9] L. Müller et al., in Proceedings of the "15th International Workshop on ECR Sources", Jyväskylä, Finland, June 2002, p.35, DOI: 10.13140/RG.2.2.17840.15361.

[10] A. Heinen and H.J. Andrä, ibid., p. 85, DOI:10.13140/RG.2.2.32100.78726.

[11] L. Müller, A. Heinen, H.W. Ortjohann, and H.J. Andrä, Rev.Sci.Instr. 73, 1140 (2002).

[12] L. Müller, B. Albers, A. Heinen, M. Kahnt, L. Nowack, H.W. Ortjohann, A. Täschner, Ch. Vitt, S. Wolosin, and H.J. Andrä, Proceedings of the ECRIS08 Workshop, Chicago, Sept 15-18, (2008), DOI: 10.13140/2.1.1584.8001.

[13] H.J. Andrä, Ibid., DOI: 10.13140/2.1.2490.5287.